Onset of Free Convection in Solutions with Variable Soret Coefficients

A. Mojtabi[1], J. K. Platten[2], M.-C. Charrier-Mojtabi[1]
[1]University Paul Sabatier, UMR CNRS INP-UPS, Toulouse, France
[2]University of Mons-Hainaut, Belgium

Abstract

It is not unusual for a Soret coefficient to change sign with temperature. We develop the theory for the onset of convection in such systems, heated from below or from above, provided that the mean temperature is precisely that at which the change of sign occurs. We also consider the realistic case of rigid, conducting, impervious boundaries for later comparison with laboratory experiments.

1. Introduction

The Soret coefficient D_T/D of an aqueous solution of NaCl (0.5 M/1) has unusual behaviour [1], being negative below 12 °C and positive above. If a solution, initially homogeneous in composition is heated from below, the Soret effect will induce a vertical concentration distribution that will drastically modify the condition for the onset of free convection. When the mean temperature of the system T_0 is maintained at 12 °C, then, in the lower hot part, the Soret coefficient is positive and salt migrates towards the cold, i.e. upwards. On the contrary, in the upper cold part the Soret coefficient is negative and the solute goes towards the hot side, i.e. downwards. In a certain sense, the solute is concentrated in the middle part of the layer, with the top-cold and bottom-hot parts having lower salt concentrations. Alternatively, one could heat the solution from above. Now, the upper part being hot, the Soret coefficient is positive and salt migrates to the cold region, i.e. downwards. In the lower, cold part, the Soret coefficient is negative and salt migrates to the hot region, i.e. upwards. Here too, the solute is concentrated in the middle of the layer. Thus, in both cases, convection may arise since a more concentrated solution lies on top of a less concentrated solution at the lower boundary, independent of the temperature gradient, normal or adverse. To be complete, one could also consider a solution for which the Soret coefficient is positive below some characteristic temperature T_0, and negative

above T_0. Examples are found in water-ethanol systems for which $D_T/D > 0$ at a given mass fraction (e.g. $N_1^0 \approx 0.27$ in ethanol) decreases with T and could become negative at high temperatures [2]. In such a case the opposite effect is observed: the denser component leaves the middle of the layer and the solution becomes more concentrated in the heavier component near the boundaries. This could also induce convection at the most unexpected time, since a top-heavy solution rests on the middle layer, where the denser component is less concentrated. We will show that the steady concentration profile of the heavier component is parabolic, instead of being linear as in all previous studies [3]. The goal of this paper is to study the influence of such a parabolic concentration profile on the onset of free convection and later to compare with laboratory experiments using Laser Doppler velocimetry to detect convection. Therefore we adopt realistic boundary conditions: rigid, conducting and impervious, as in an experimental cell with lower and upper boundaries made of copper plates.

2. Formulation of the problem

The starting point will be the conservation equations for an incompressible fluid in the "partial" Boussinesq approximation

$$\nabla \cdot \vec{V} = 0 \tag{1}$$

$$\rho_0 \left(\frac{\partial \vec{V}}{\partial t} + \vec{V} \cdot \nabla \vec{V} \right) = -\nabla p + \mu \nabla^2 \vec{V} + \rho_0 [-\alpha (T - T_0) + \beta (N_1 - N_1^0)] \vec{g} \tag{2}$$

$$\rho_0 C_p \left(\frac{\partial T}{\partial t} + \vec{V} \cdot \nabla T \right) = \lambda \nabla^2 T \tag{3}$$

$$\rho_0 \left(\frac{\partial N_1}{\partial t} + \vec{V} \cdot \nabla N_1 \right) = \nabla \cdot (\rho_0 D \nabla N_1 + \rho_0 D_T N_1^0 N_2^0 \nabla T). \tag{4}$$

Notations are conventional; here N_1 represents the mass fraction of the denser component, of mean value N_1^0, such that the mass expansion coefficient β is positively defined:

$$\beta = \frac{1}{\rho_0} \frac{\partial \rho}{\partial N_1} > 0 \tag{5}$$

and $N_2^0 = 1 - N_1^0$.

By "partial" Boussinesq approximation we mean that the thermal diffusion coefficient D_T in Eq. (4) is temperature dependent, and we will take a linear law:

$$\frac{D_T}{D} = \mathscr{D}(T - T_0). \tag{6}$$

The slope $\mathscr{D}$ may be either negative or positive. Obviously, the change of sign of the Soret coefficient D_T/D is solely due to D_T, since the isothermal diffusion coefficient D

is strictly positive. Therefore D will be considered as a constant in the Boussinesq approximation.

We now take, for the length scale, the depth h of the liquid layer; for the velocity scale, a/h where a is the thermal diffusivity $\lambda/\rho_0 C_p$; for pressure $\rho_0 a^2/h^2$; and for time h^2/a. The non-dimensional temperature is defined by $(T - T_0)/\Delta T_0$ where $T_0 = \dfrac{T_l + T_u}{2}$, $\Delta T_0 = T_l - T_u$ where T_l is the temperature of the lower plate (at $z = 0$) and T_u that of the upper plate (at $z = 1$). Thus $\Delta T_0 > 0$ for a bottom heated system and $\Delta T_0 < 0$ for a top heated system.

The new mass fraction is defined by $(N_1 - N_1^0)/N_1^0 N_2^0$. We shall not use new symbols (e.g. primed symbols) for nondimensional quantities. Eqs (1)–(4) become ($\vec{k}$ is the unit upward vector)

$$\nabla \cdot \vec{V} = 0 \tag{7}$$

$$\frac{\partial \vec{V}}{\partial t} + \vec{V} \cdot \nabla \vec{V} = -\nabla p + \mathrm{Pr} \nabla^2 \vec{V} + \mathrm{Pr}(Ra_T T - Ra_s N_1)\vec{k} \tag{8}$$

$$\frac{\partial T}{\partial t} + \vec{V} \cdot \nabla T = \nabla^2 T \tag{9}$$

$$\frac{\partial N_1}{\partial t} + \vec{V} \cdot \nabla N_1 = \frac{1}{Le} \nabla \left(\nabla N_1 + \frac{D_T}{D} \Delta T_0 \cdot \nabla T \right). \tag{10}$$

Here Pr is the usual Prandtl number and Ra_T is the thermal Rayleigh number (positive when the system is heated from below and negative when the system is heated from above), whereas Ra_s is analogous to a solutal Rayleigh number

$$Ra_s = \frac{g \beta N_1^0 N_2^0 h^3}{a \nu}. \tag{11}$$

Finally Le is the Lewis number defined by

$$Le = \frac{a}{D} = \frac{\nu/D}{\nu/a} = \frac{Sc}{Pr}, \tag{12}$$

where $Pr = \nu/a$ is the Prandtl number already mentioned and Sc is the Schmidt number. In a liquid phase, since the thermal diffusivity is much higher than the mass diffusivity, a value of $Le \approx 100$ seems quite reasonable.

Using Eq. (6) for D_T/D, written with a nondimensional temperature, Eq. (10) becomes

$$\frac{\partial N_1}{\partial t} + \vec{V} \cdot \nabla N_1 = \frac{1}{Le} \nabla \cdot (\nabla N_1 + ST \cdot \nabla T) \tag{10'}$$

$$= \frac{1}{Le} [\nabla^2 N_1 + ST \cdot \nabla^2 T + S(\nabla T)^2] \tag{10''}$$

where $S = \mathscr{D}(\Delta T_0)^2$ represents the contribution of the Soret effect through the slope $\mathscr{D}$ of $\dfrac{D_T}{D}$. Let us once again emphasize that $\mathscr{D} > 0$ or $\mathscr{D} < 0$.

In order to solve Eqs. (7)–(10) or (10′) or (10″) we adopt realistic boundary conditions: no slip, prescribed temperature and zero mass flux at the boundaries:

$$\begin{aligned} &\text{At } z = 0\text{: } \vec{V} = 0; T = 1/2; \frac{\partial N_1}{\partial z} + \frac{S}{2}\frac{\partial T}{\partial z} = 0 \\ &\text{At } z = 1\text{: } \vec{V} = 0; T = -1/2; \frac{\partial N_1}{\partial z} - \frac{S}{2}\frac{\partial T}{\partial z} = 0. \end{aligned} \tag{13}$$

3. Steady conductive state

To the motionless state $\vec{V} = 0$, corresponds a mass fraction profile $\bar{N}_1$, a temperature profile $\bar{T}$, a pressure $\bar{p}$, and solutions of

$$-\nabla\bar{p} + Pr(Ra_T\bar{T} - Ra_s\bar{N}_1)\vec{k} = 0 \tag{14}$$

$$\nabla^2\bar{T} = 0, \ \textit{or } \bar{T} = 1/2 - z \tag{15}$$

$$\nabla\cdot(\nabla\bar{N}_1 + S\bar{T}\nabla\bar{T}) = 0. \tag{16}$$

Thus, as already written in the boundary conditions (13), the temperature of the lower boundary in a reduced form is always 1/2, and that of the upper boundary is – 1/2, independent of the direction of heating, which only affects the sign of the Rayleigh number Ra_T. At the steady state (zero mass flux across the layer), Eq. (16) and the temperature distribution (15), imply

$$\frac{\partial\bar{N}_1}{\partial z} - S(1/2 - z) = 0 \tag{17}$$

from which the steady mass fraction distribution is deduced,

$$\bar{N}_1 = \frac{S}{2}(-1/6 + z - z^2), \tag{18}$$

the integration constant of (17) being determined by the additional condition

$$\int_0^1 \bar{N}_1(z)dz = 0. \tag{19}$$

At the two boundaries $z = 0$ and $z = 1$, we have

$$\bar{N}_1(0) = \bar{N}_1(1) = -\frac{S}{12}$$

and in the centre of the cavity

$$\bar{N}_1(1/2) = +\frac{S}{24}.$$

This exactly describes the enrichment of the center of the cavity in component 1 (the heavier) at the expense of the boundaries when $S > 0$, or the depletion of component 1 in the center when $S < 0$; in the latter case, the boundaries are enriched in component 1. This has been discussed qualitatively in the introduction. Finally, from Eq. (14) the pressure field $\bar{p}(z)$ (cubic) could be deduced, but this will not be done here.

4. Linearized equations and boundary conditions

The steady solution described in the previous paragraph can be perturbed

$$\vec{V} = 0 + \vec{v}; \quad p = \bar{p} + \pi; \quad T = \bar{T} + \vartheta; \quad N_1 = \bar{N}_1 + n_1 \tag{20}$$

and the equations are linearized into the disturbances $\vec{v}, \pi, \vartheta$ and n_1, all dependent on time and space:

$$\nabla \cdot \vec{v} = 0 \tag{21}$$

$$\frac{\partial \vec{v}}{\partial t} = -\nabla\pi + Pr\,\nabla^2\vec{v} + Pr(Ra_T\vartheta - Ra_s n_1)\vec{k} \tag{22}$$

$$\frac{\partial \vartheta}{\partial t} + \vec{v}\cdot\nabla\bar{T} = \nabla^2\vartheta \tag{23}$$

$$\frac{\partial n_1}{\partial t} + \vec{v}\cdot\nabla\bar{N}_1 = \frac{1}{Le}(\nabla^2 n_1 + S\bar{T}\nabla^2\vartheta + 2S\nabla\vartheta\cdot\nabla\bar{T}). \tag{24}$$

Taking twice the curl of Eq. (22) in order to eliminate the pressure π, using the notation W for the vertical component of $\vec{v}$ and $\nabla^2_{x,y}$ for the Laplace operator in the horizontal plane, $\nabla^2_{x,y} = \dfrac{\partial^2}{\partial x^2} + \dfrac{\partial^2}{\partial y^2}$, we get

$$\frac{1}{Pr}\frac{\partial}{\partial t}\nabla^2 W = Ra_T\nabla^2_{x,y}\vartheta - Ra_s\nabla^2_{x,y}n_1 + \nabla^4 W \tag{25}$$

$$\frac{\partial \vartheta}{\partial t} - W = \nabla^2\vartheta \tag{26}$$

$$\frac{\partial n_1}{\partial t} + WS\left(\frac{1}{2} - z\right) = \frac{1}{Le}\left[\nabla^2 n_1 + S\left(\frac{1}{2} - z\right)\nabla^2\vartheta - 2S\frac{\partial\vartheta}{\partial z}\right]. \tag{27}$$

The normal mode analysis $(W, \vartheta, n_1) = (W(z), \vartheta(z), n_1(z))e^{i(k_x x + k_y y)}e^{\sigma t}$ leads to

$$(k^2 = k_x^2 + k_y^2; D = d/dz)$$

$$\frac{\sigma}{Pr}\left(D^2 - k^2\right)W = -k^2(Ra_T\vartheta - Ra_s n_1) + \left(D^2 - k^2\right)^2 W \tag{28}$$

$$\sigma\vartheta - W = \left(D^2 - k^2\right)\vartheta \tag{29}$$

$$\sigma n_1 + WS\left(\frac{1}{2} - z\right) = \frac{1}{Le}\left[(D^2 - k^2)n_1 + S\left(\frac{1}{2} - z\right)(D^2 - k^2)\vartheta - 2SD\vartheta\right]. \tag{30}$$

In a first step, we restrict ourselves not only to marginal stability $\sigma = 0 + i\omega$, but also to the non-oscillatory marginal stability $\omega = 0$. We shall come back to this point later in order to verify this strong hypothesis.

Subsequently, Eqs. (28)–(30) reduce to

$$(D^2 - k^2)^2 W - k^2 Ra_T\vartheta + k^2 Ra_s n_1 = 0 \tag{31}$$

$$(D^2 - k^2)\vartheta + W = 0 \tag{32}$$

$$(D^2 - k^2)n_1 - LeS\left(\frac{1}{2} - z\right)W + S\left(\frac{1}{2} - z\right)(D^2 - k^2)\vartheta - 2SD\vartheta = 0. \tag{33}$$

The natural boundary conditions for rigid and perfectly conducting walls are

$$W = DW = \vartheta = 0 \text{ at } z = 0 \text{ and } 1 \tag{34}$$

associated with boundary conditions for n_1, deduced from Eq. (13), namely

$$\begin{aligned} Dn_1 + \frac{S}{2}D\vartheta &= 0 \text{ at } z = 0 \\ Dn_1 - \frac{S}{2}D\vartheta &= 0 \text{ at } z = 1. \end{aligned} \tag{35}$$

These boundary conditions are ''non-symmetrical''. Therefore we define a new field ζ by:

$$S\zeta = n_1 + S\left(\frac{1}{2} - z\right)\vartheta \tag{36}$$

such that the boundary conditions (35) are transformed into

$$D\zeta = 0 \text{ at } z = 0 \text{ and } 1. \tag{37}$$

With this new field, differential equations (31)–(33) are transformed into

$$(D^2 - k^2)^2 W - k^2 \left[Ra_T + R_S \left(\frac{1}{2} - z \right) \right] \vartheta + k^2 R_S \zeta = 0 \tag{38}$$

$$(D^2 - k^2)\vartheta + W = 0 \tag{39}$$

$$(D^2 - k^2)\zeta - Le \left(\frac{1}{2} - z \right) W = 0 \tag{40}$$

$$W = DW = \vartheta = D\zeta = 0 \text{ at } z = 0 \text{ and } 1, \tag{41}$$

where R_S stands for the product $Ra_s\ S$:

$$R_S = \frac{g\beta N_1^0 N_2^0 h^3 \mathscr{D} \Delta T_0^2}{a\nu}. \tag{42}$$

5. Galerkin technique, trial functions and numerical results

A very simple choice for W, ϑ and ζ satisfying the conditions (41) could be

$$W = \sum_{i=1}^{N} A_i \sin \pi z \sin i\pi z \tag{43}$$

$$\vartheta = \sum_{i=1}^{N} B_i \sin i\pi z \tag{44}$$

$$\zeta = \sum_{i=1}^{N} C_i \cos(i-1)\pi z. \tag{45}$$

The reason for the expansion in $\cos(i-1)\pi z$ is to consider a constant term C_1 in ζ. The application of the Galerkin technique is classical, and no more details will be given here. The MAPLE software was used for the symbolic calculations of the residues and of the $3N \times 3N$ determinant.

Without the thermodiffusion effect ($R_S = 0$) we already find with $N = 2$, $Ra_T^{crit} = 1825$, i.e. a discrepancy of only 7% from the exact value 1708. This accuracy is sufficient, considering the experimental error on a Rayleigh number which is of the same order of magnitude (say 1% on each of the parameters $\alpha, \Delta T, h, a$ and ν). We have calculated the variation of the critical point with R_S. However, results will not be given here with the trigonometric sets.

Indeed, it is well known from the usual Benard problem that a polynomial expansion yields a much better result, namely $Ra_T^{crit} = 1750$ instead of 1825 at the lowest level of

approximation, and that the convergence of Ra_T^{crit} is much faster. Therefore the following set is more suitable:

$$W = \sum_{i=1}^{N} A_i z^2 (1-z)^2 \left(z - \frac{1}{2}\right)^{i-1} \tag{46}$$

$$\vartheta = \sum_{i=1}^{N} B_i z (1-z) \left(z - \frac{1}{2}\right)^{i-1} \tag{47}$$

$$\zeta = C_1 + C_2 \left(1 - \frac{3}{2}z^2 + z^3\right) + \sum_{i=3}^{N} C_i z^2 (1-z)^2 \left(z - \frac{1}{2}\right)^{i-3}. \tag{48}$$

In writing a polynomial expansion for ζ, we take care that $\zeta \neq 0$ at the boundaries by putting a constant C_1, and that the lowest approximation such that $D\zeta = 0$ ($z = 0$ and 1) is cubical $\zeta \doteqdot \left(1 - \frac{3}{2}z^2 + z^3\right)$. This justifies the choice (48).

Three approximations were used, namely $N = 2, 4$ and 6, since at each higher approximation, we want to add an odd and an even function for W, ϑ and ζ. Indeed the eigenfunctions do not fall into two noncombining groups of even and odd functions owing to the $\left(\frac{1}{2} - z\right)$ term in differential equations (38)–(40). At each level of approximation the symbolic calculation of the $3N \times 3N$ determinant was achieved using the MAPLE software. Then, terms in the different powers of R_S were collected. We verified that only even powers of R_S were present in the determinants. This implies that opposite values of R_S would produce the same critical thermal Rayleigh number. In other words, the critical Rayleigh number is symmetrical with respect to the $R_S = 0$ line.

Numerical results are listed in Table 1 and the converged values are displayed in Figure 1 only up to $|R_S| = 350$ (the paths Oa, Ob, Oa′,Ob′ correspond to experiments – see discussions § 6 below). From the computed points shown in Figure 1, the variation of Ra_T is (to a good approximation) given by:

$$Ra_T^{crit} = 1705.2 - 3.6741\,10^{-2} R_S^2 + 1.2375\,10^{-8} R_S^4. \qquad (Le = 100) \tag{49}$$

This is sufficient for comparison between experiments, since for $R_S = 0$ we find $Ra_T^{crit} = 1705.2$ instead of 1708. A lower approximation (i.e. parabolic) is less suitable because it gives $Ra_T^{crit} = 1687$ for $R_S = 0$. Before ending this paragraph concerned with numerical results, we would like to come back to the hypothesis of non-oscillatory marginal stability $\sigma = 0$. First of all, in the two-component Benard problem with constant Soret coefficient [3], the first bifurcation may be non-oscillatory or, on the contrary, of Hopf type, depending on the sign of D_T/D. When $D_T/D > 0$, a destabilizing case when the system is heated from below, it has been demonstrated that the principle of exchange of stability holds. However, when $D_T/D < 0$, a stabilizing effect when the system is heated from below, a Hopf bifurcation characterized by its frequency ω, is observed provided that $|D_T/D|$ exceeds a given value. Remembering also the Benard problem with rotation or with a magnetic field [4], the critical Rayleigh number increases with the so-called Taylor number measuring the Coriolis

Table 1. Relation between R_s and Ra_T on the neutral stability curve, together with critical wavenumber. $Le = 100$.

	$N = 2$		$N = 4$		$N = 6$	
R_s	Ra_T^{crit}	k^{crit}	Ra_T^{crit}	k^{crit}	Ra_T^{crit}	k^{crit}
0	1749.98	3.117	1708.55	3.117	1707.762	3.117
10	1746.62	3.12	1704.82	3.12	1704.04	3.116
40	1696.79	3.10	1648.92	3.11	1648.24	3.11
60	1630.55	3.09	1574.58	3.10	1574.03	3.10
100	1419.94	3.05	1338.14	3.06	1337.86	3.06
140	1107.76	2.98	987.28	3.01	987.06	3.01
160	914.72	2.94	770.08	2.97	769.72	2.97
180	697.68	2.90	525.65	2.94	525.00	2.94
200	457.13	2.85	254.45	2.89	253.32	2.89
220	193.50	2.79	-43.12	2.85	−44.94	2.85
240	−92.78	2.74	−336.71	2.80	−369.42	2.80
260	−401.39	2.68	−716.02	2.74	−719.85	2.74
280	−732.02	2.62	−1090.83	2.68	−1096.00	2.69
300	−1084.00	2.55	−1490.99	2.62	−1497.70	2.63
350	−2059.62	2.38	−2601.87	2.46	−2613.17	2.47
400	−3168.65	2.22	−3870.86	2.30	−3887.50	2.31
450	−4411.80	2.06	−5299.33	2.15	−5321.67	2.16
500	−5789.78	1.91	−6889.10	2.00	−6917.21	2.01
600	−8956.37	1.65	−10558.90	1.75	−10598.18	1.76
700	−12676.44	1.44	−14889.82	1.55	−14939.34	1.55
1000	−27206.00	1.03	−31884.45	1.13	−31960.08	1.13

forces, or the so-called Hartmann number measuring the intensity of the Lorentz force. In both cases "overstability" (using the old nomenclature of Chandrasekhar), or a Hopf bifurcation is found, but once more provided that the stabilizing forces exceed a given value, itself depending on the Prandtl number. Summarizing, an oscillatory onset of convection in liquid layers heated from below is observed, in all cases studied up to now, only when a stabilizing force is applied. In the problem studied in the present paper, the Soret effect has a destabilizing effect, and therefore a Hopf bifurcation is not expected on the basis of the preceding observations, but of course this is not a proof. Therefore in Eqs. (28)–(30) we leave σ as a possible complex eigenvalue and next we use the new field ζ defined in Eq. (36). As a matter of fact, Eqs. (38)–(40) will be modified. They now read

$$(D^2 - k^2)^2 W - \frac{\sigma}{Pr}(D^2 - k^2)W + k^2\left[Ra_T + R_S\left(\frac{1}{2} - z\right)\right]\vartheta + k^2 R_S \zeta = 0 \tag{50}$$

$$(D^2 - k^2 - \sigma)\vartheta + W = 0 \tag{51}$$

$$(D^2 - k^2 - \sigma Le)\zeta + \sigma Le\left(\frac{1}{2} - z\right)\vartheta - Le\left(\frac{1}{2} - z\right)W = 0. \tag{52}$$

We now use the same Galerkin technique and the same expansions as before. The new determinant is a function of Ra_T, R_S, k, Le and σ, the goal being eventually to find an

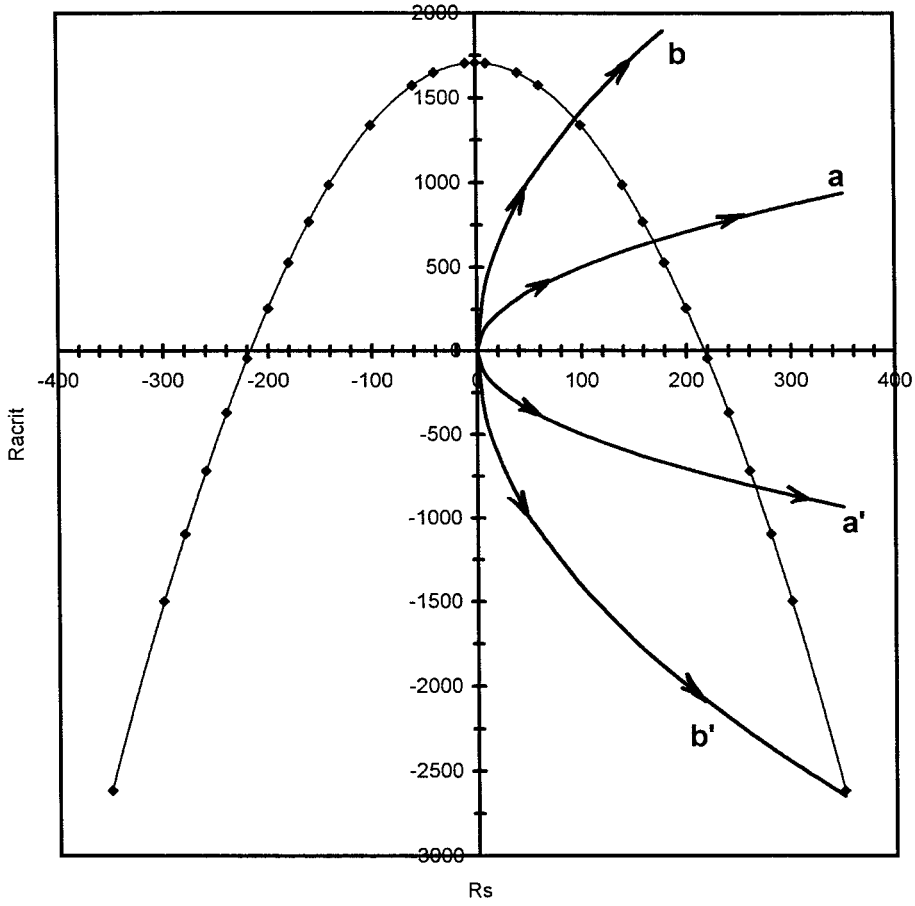

Fig. 1. Variation of Ra_T^{crit} with R_S for $Le = 100$.

oscillatory instability $\sigma = 0 + i\omega$ at a Rayleigh number Ra_T smaller than that at which non-oscillatory marginal stability $\sigma = 0$ is observed.

Thus, at prescribed values of R_S, Le and k we scanned a large range of thermal Rayleigh numbers (from zero up to several tens of thousands) and asked for all the eigenvalues σ at a given level of approximation in the Galerkin technique. The most dangerous eigenvalue, i.e. with a real part changing sign when scanning a very large range of Ra_T, was always real. Some complex conjugate roots $\sigma = \sigma_R \pm i\omega$ did appear, but always with a negative real part. Thus we conclude that we possess "numerical proof" of non-oscillatory marginal stability.

6. Discussion

In any experiment, we start with the equilibrium state, i.e. no temperature difference, with a mean temperature such that $D_T/D = 0$ (e.g. 12 °C for a 0.5M/1 NaCl aqueous

solution). The temperature difference is increased by steps. That means that in one experiment we follow (Figure 1) the parabolic path Oa or Ob when we heat from below, depending on the spacing h together with the values of the physical parameter of the solution (or Oa′ or Ob′ if we heat from above) since, due to the ΔT_0^2 in R_S, the latter parameter increases more rapidly than Ra_T. The intersection of the different paths with the critical curve gives the experimental critical points $(Ra_T^{crit}, R_S^{crit})$ with a critical thermal Rayleigh number always smaller than 1707.762 if we heat from below. When we heat from above $(Ra_T < 0)$ the absolute value of Ra_T^{crit} may be very large (very negative, like in an experiment described by the path Ob′) since the destabilizing solute gradient (more or less pronounced) has to oppose a stabilizing temperature gradient. On the other hand, we would like to define a non dimensional parameter characterizing the Soret effect in our particular situation, which does not contain the imposed temperature gradient (as is the case with R_S), which only reflects the physical properties of the solution similar to the separation ratio ψ for systems with constant Soret coefficient D_T/D and defined as:

$$= \frac{\beta}{\alpha} N_1^0 N_2^0 \frac{D_T}{D}. \tag{53}$$

Let us recall here that this separation ratio represents the contribution of the salt gradient $\beta\Delta\bar{N}_1/h$ to the density gradient $\Delta\rho$, relative to the contribution of the temperature gradient $-\alpha\Delta\bar{T}/h$:

$$= -\frac{\beta\Delta\bar{N}_1}{\alpha\Delta\bar{T}}, \tag{53 bis}$$

where $\Delta\bar{N}_1/\Delta\bar{T} = -N_1^0 N_2^0 D_T/D$.

Here, we may not simply replace D_T/D by $\mathscr{D}(T - T_0)$ in (53) because T is space dependent. From dimensional arguments, there must exist a non-dimensional quantity:

$$= \frac{\beta}{\alpha} N_1^0 N_2^0 \mathscr{D} \cdot T_{réf} \tag{54}$$

that characterizes the Soret effect, in which a suitable "reference temperature" T_{ref} is representative of the physical parameters of the solution, and not dependent on the imposed temperature gradient which is continuously varied in an experiment. It seems that $T_{ref} = a\nu/\alpha g h^3$ is a good choice. Thus we generalize the notion of separation ratio in our problem by defining

$$= \frac{\beta}{\alpha} N_1^0 N_2^0 \mathscr{D} \frac{a\nu}{\alpha g h^3}. \tag{55}$$

We arrive at the same conclusion considering that Ra_T is proportional to ΔT_0 and R_S is proportional to ΔT_0^2. It follows that R_S is proportional to Ra_T^2. Let us write:

$$R_S = Ra_T^2 \cdot \quad . \tag{56}$$

If we put the definition of R_S and Ra_T into (56), then definition (55) for ψ is found again. In other words, this simply means that we could use other scalings for the dimensional quantities than the ones used in Sect. 2. In particular we could scale the temperature not by ΔT_0, but by $a\nu/g\alpha h^3$, and the mass fraction by $a\nu/g\beta h^3$. These scalings were adopted by Lücke's group for example [5]. With these new scales, it may be verified that Eqs. (7) and (9) are unaffected, whereas Eqs. (8) and (10″) become

$$\frac{\partial \vec{V}}{\partial t} + \vec{V} \cdot \nabla \vec{V} = -\nabla p + Pr \nabla^2 \vec{V} + Pr(T - N_1)\vec{k} \tag{57}$$

$$\frac{\partial N_1}{\partial t} + \vec{V} \cdot \nabla N_1 = \frac{1}{Le}[\nabla^2 N_1 + \psi T \cdot \nabla^2 T + \psi(\nabla T)^2]. \tag{58}$$

In these new equations the thermal Rayleigh number has disappeared, but is now in the steady temperature gradient such that: $\frac{\partial \bar{T}}{\partial z} = -1$ is replaced by $\frac{\partial \bar{T}}{\partial z} = -Ra_T$ and thus the thermal Rayleigh number is reintroduced into the perturbation equations via the nonlinear term $\vec{V} \cdot \nabla T$ in the energy equation instead of in the momentum equation. We do not feel it is necessary to reformulate the eigenvalue problem, so we simply use the transformation (56) in Eq. (49), and get a good approximation (i.e. for $-3000 < Ra_T < +1750$).

$$-1.2375\,10^{-8} Ra_T^{8} \;^{4} + 3.6741\,10^{-2} Ra_T^{4} \;^{2} + Ra_T - 1750 = 0. \quad (Le = 100) \tag{59}$$

For any value of Ψ, we find the two interesting (i.e. the smallest in modulus) real roots for Ra_T (one positive that tends to 1705 when $\Psi \to 0$, and one negative that tends to $-\infty$ when Ψ becomes small). These two roots are given in Table 2. Thus we may easily transform Figure 1 into Figure 2, more appropriate for comparison with

Table 2. Variation of critical thermal Rayleigh numbers with ψ.

	$Ra_T^{(2)}$	$Ra_T^{(1)}$
0.00000	–	1705.0
0.00001	−7178.0	1676.0
0.00002	−4630.0	1607.0
0.00004	−3031.0	1448.0
0.00006	−2381.0	1313.0
0.00008	−2012.0	1208.0
0.00010	−1768.0	1123.0
0.00020	−1193.0	869.0
0.00040	−813.9	652.2
0.00060	−653.5	545.6
0.00080	−560.1	479.2
0.00100	−497.4	432.7

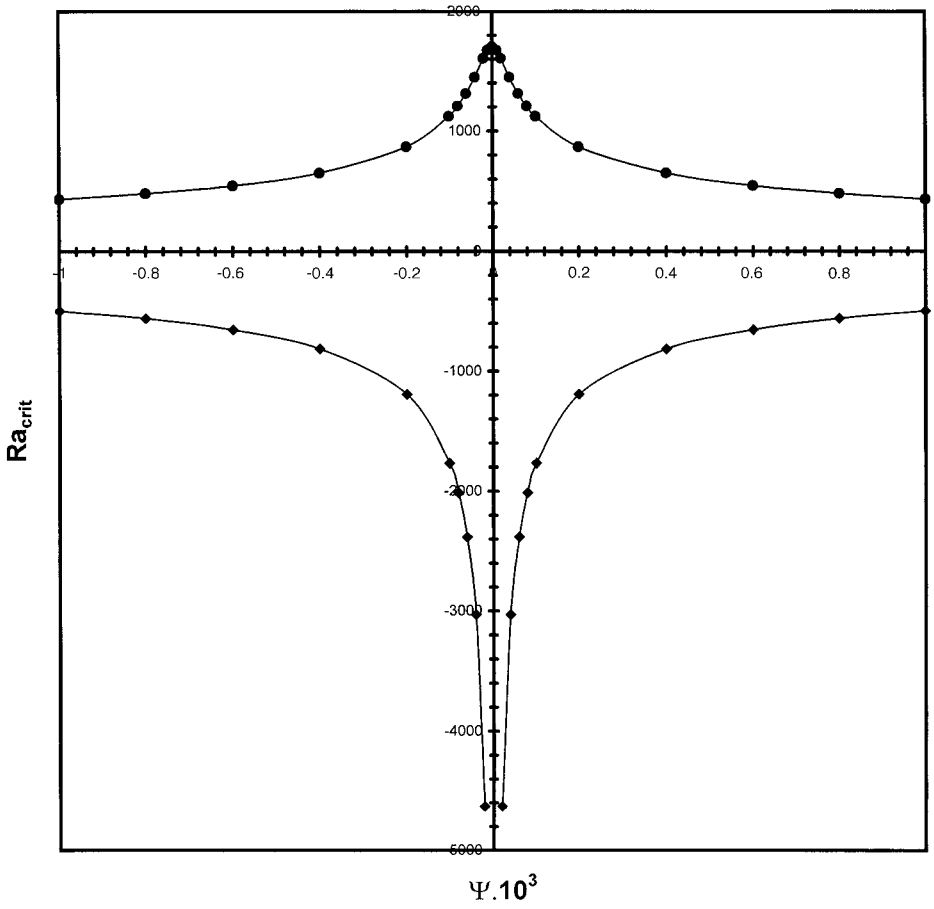

Fig. 2. Variation of Ra_T^{crit} with ψ for $Le = 100$.

experiments. Indeed, for a given solution, Ψ may be computed from the knowledge of the physical properties. Next the two critical thermal Rayleigh numbers are deduced from Eq. (59).

7. Experimental relevance

Let us now proceed to some estimations concerning the critical temperature difference in experiments on the onset of convection in H_2O-NaCl (0.5 M/1) solutions, compared to what is expected in pure water, all the experiments being conducted at a mean temperature of 12 °C.

The following properties at $To = 12\,^{\circ}\mathrm{C}$ are found in tables [6] for pure water:
Density: $\rho = 0.9994974\,\mathrm{g/cm^3}$
Viscosity: $\mu = 1.235 \times 10^{-2}\,\mathrm{g/cm \cdot sec}$
Kinematic viscosity: $\nu = 1.236 \times 10^{-2}\ \mathrm{cm^2/sec}$

Thermal conductivity: $\lambda = 5.83 \times 10^{-3}$ Joule/sec $\cdot$ cm $\cdot$ K
Specific heat: $C_p = 4.1893$ Joule/g $\cdot$ K
Thermal diffusivity: $a = 1.392 \times 10^{-3}$ cm^2/sec
Prandtl number: $Pr = \dfrac{\nu}{a} = 8.9$
Expansion coefficient: $\alpha = \dfrac{1}{\rho}\dfrac{\partial \rho}{\partial T} = 1.1408 \times 10^{-4}\,\mathrm{K}^{-1}$.

Therefore we estimate the Rayleigh number as:

$Ra_T = 6504.6 \times \Delta T \times h^3$

or from its critical value $Ra_t^{crit} = 1708$

$\Delta T^{crit} \cdot h^3 = 0.26258(^\circ\mathrm{C} \cdot \mathrm{cm}^3)$.

Thus, a 4-mm-deep layer would give $\Delta T^{crit} = 4.1\,^\circ$C, a very convenient value to verify and compatible with a Boussinesq approximation since the cold plate would be at a temperature close to 10 °C, thus far from 4 °C where the expansion coefficient of pure water vanishes.

Concerning the salt solution, most values were taken from tables [6], followed by interpolation, simply because the required quantities are not given exactly at 12 °C, but rather at 5, 10, 15, 20 °C etc. Also the mean mass fraction of salt ($N_1^0 = 0.0287$, corresponding to 0.5 M/1 or 29.25 gr/1) is such that the physical parameters are not given at this precise mass fraction or concentration. We have found relevant parameters in tables at different *molalities* in mol/kg of water, as e.g.: 0.1; 0.25; 0.5; 0.75 etc.

Thus, one has to interpolate between values given in tables and this can be dangerous, not so much for the primary properties like viscosity, thermal conductivity, density, but certainly for their derivatives, in particular the two expansion coefficients α and β. Therefore the densities, and consequently the expansion coefficients, were measured in our lab using a vibrating quartz U tube densitometer manufactured by PAAR with a resolution of 10^{-6} g/cm^3. The solution was prepared by weighing 2.87 g NaCl and 97.13 g water, corresponding exactly to a salt mass fraction of $N_1^0 = 0.0287$ and a concentration of 0.5 M/1. The following densities were obtained:

T(°C)	$\rho(g/\mathrm{cm}^3)$
11	1.020485
11.5	1.020398
12	1.020308
12.5	1.020214
13	1.020118

Thus $\alpha = (18.00 \pm 0.16)10^{-5}\,\mathrm{K}^{-1}$.

Similarly, by changing the mass fraction of salt slightly, keeping $To = 12\,^\circ$C

$$\beta = \frac{1}{\rho_0}\left(\frac{\partial \rho}{\partial N_1}\right)_{T=12} = 0.718.$$

Let us note that the thermal expansion coefficient of the salt solution is 50% higher than that of pure water, owing to the fact that the density maximum at 4 °C disappears for the salt solution. Vergaftik [6] gives the viscosity of NaCl solution with mass fractions from 5% to 25% between −10 °C and +80 °C. Interpolation is thus possible:

$\mu = 1.28$ cp or $\nu = 0.0125\,\mathrm{cm}^2/\mathrm{sec}$. The dynamic viscosity μ increases by $\approx 4\%$ due to the addition of salt, but so does the density. As a consequence, the kinematic viscosity is almost unchanged.

The thermal conductivity λ can be estimated from the International Critical Tables

$$\lambda\big(T, N_1^0\big) = \lambda_0(T)\big(1 - 248 \cdot 10^{-5} \cdot N_1^0\big),$$

where $\lambda_0(T)$ is the temperature dependent thermal conductivity of pure water.

Finally for the solution at 12 °C:
$\lambda = 0.0058$ watt/cmK (almost the same as pure water)

$C_p = 4.023$ J/gr K

and $a = 0.00141\,\mathrm{cm}^2/\mathrm{sec}$.

The last parameter still to be estimated is $\mathscr{D}$ (cf Eq. (6)). From figure 4 of Ref [1], we estimate with reasonable accuracy:

$$\frac{D_T}{D} \approx -0.001\,\mathrm{K}^{-1} \quad \text{at } T = 2\,^\circ\mathrm{C}$$

$$\frac{D_T}{D} \approx +0.001\,\mathrm{K}^{-1} \quad \text{at } T = 23\,^\circ\mathrm{C}$$

and therefore:

$$\mathscr{D} = \frac{0.002}{21} = 0.95\,10^{-4}\,\mathrm{K}^{-2}.$$

We are now able to estimate the parameter ψ defined by Eq. (55) for a 4 mm layer

$$= 1.6475 \times 10^{-5}.$$

One has also to keep in mind that the Lewis number Le is not exactly 100 for the salt solution and therefore the results presented in Table 1 cannot be used for the salt solution. The isothermal diffusion coefficient is estimated to be:

$$D = 1.00207\,10^{-5}\,\mathrm{cm}^2/\mathrm{sec}.$$

Therefore,

$$Le = \frac{1.41\,10^{-3}}{1.00207\,10^{-5}} \approx 140.7.$$

Table 3. Relation between R_S and Ra_T on the neutral stability curve, together with critical wavenumber. $Le = 140$.

$Le = 140$	$N = 2$		$N = 4$		$N = 6$		$N = 8$	
R_S	Ra_T^{crit}	k^{crit}	Ra_T^{crit}	k^{crit}	Ra_T^{crit}	k^{crit}	Ra_T^{crit}	k^{crit}
0	1749.976	3.116	1708.550	3.116	1707.762	3.116	1707.762	3.116
10	1743.50	3.115	1701.28	3.115	1700.50	3.115	1700.50	3.11
40	1646.55	3.094	1592.41	3.099	1591.85	3.099	1591.83	3.10
60	1518.00	3.067	1447.99	3.078	1447.60	3.078	1447.59	3.07
100	1111.64	2.98	991.07	2.99	990.75	3.00	990.69	3.01
140	514.48	2.86	317.85	2.90	316.97	2.90	316.66	2.90
160	147.54	2.78	−96.71	2.84	−98.72	2.84	−98.93	2.84
180	−263.45	2.70	−561.91	2.77	−565.32	2.77	−565.61	2.77
200	−717.59	2.62	−1076.99	2.70	−1082.29	2.69	−1082.70	2.69
220	−1214.20	2.53	−1641.70	2.60	−1649.13	2.61	−1649.66	2.61
240	−1752.84	2.43	−2255.61	2.51	−2265.57	2.51	−2256.26	2.52
260	−2333.24	2.34	−2918.81	2.42	−2931.62	2.43	−2932.42	2.43
280	−2955.34	2.25	−3631.44	2.33	−3647.28	2.34	−3648.22	2.34
300	−3619.20	2.16	−4393.77	2.24	−4412.77	2.25	−4413.85	2.25
350	−5462.55	1.94	−6519.13	2.03	−6546.25	2.04	−6547.66	2.04
400	−7571.02	1.75	−8961.89	1.85	−8997.00	1.86	−8998.65	1.85
450	−9947.82	1.58	−11725.74	1.68	−11767.42	1.67	−11770.28	1.68
500	−12595.45	1.45	−14813.07	1.54	−14862.96	1.55	−14865.06	1.55
600	−18714.02	1.22	−21963.32	1.32	−22026.22	1.33	−22028.54	1.33
700	−25922.57	1.05	−30417.69	1.15	−30492.39	1.12	−30482.14	1.12
1000	−54183.02	0.74	−63613.85	0.83	−63720.23	0.83	−63722.01	0.84

We recalculated Ra_T^{crit} for $Le = 140$ and the results are given in Table 3 and displayed in Figure 3 for $-3000 < Ra_T < 1750$. Instead of (59) we now have

$$-4.3843\,10^{-8}\,Ra_T^{8}\ \ ^{4} + 7.1510\,10^{-2}\,Ra_T^{4}\ \ ^{2} + Ra_T - 1705 = 0. \quad (Le = 140) \tag{60}$$

If we put the value $\psi = 1.6475 \times 10^{-5}$ corresponding to the 4 mm salt solution and solve (60) for Ra_T, we find:

$$Ra_T^{(1)} = 1583$$

$$Ra_T^{(2)} = -4242.$$

It happens that the decrease in Ra_T^{crit} from 1708 to 1583 is not so pronounced as we could have hoped (even if it corresponds to $\Delta T = 2.47\,^{\circ}\mathrm{C}$). On the other hand, the second solution (heating from above) corresponds to $\Delta T = -6.62\,^{\circ}\mathrm{C}$, a result which should be easy to check.

By decreasing the depth of the layer, one increases ψ.

Let us try a 3 mm layer, which for pure water corresponds to $\Delta T^{crit} = 9.7\,^{\circ}\mathrm{C}$. The new value is now:

$$= 3.9052 \times 10^{-5}$$

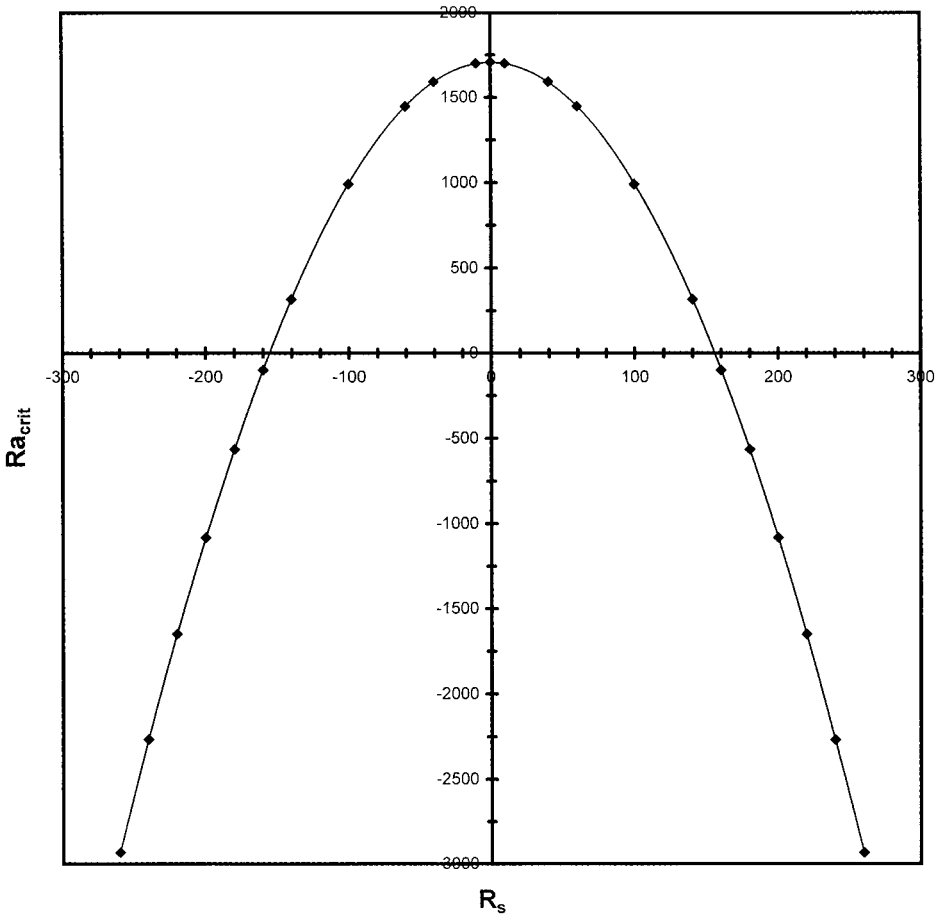

Fig. 3. Variation of Ra_T^{crit} with R_S for $Le = 140$.

and the two solutions of (60) are:

$$Ra_T^{(1)} = 1347 \quad (\Delta T = 4.98\,^\circ\mathrm{C})$$

$$Ra_T^{(2)} = -2519 \quad (\Delta T = -9.31\,^\circ\mathrm{C}).$$

And for a 2 mm layer, which for pure water gives (mathematically) $\Delta T^{crit} = 32.8\,^\circ\mathrm{C}$ (an impossible experiment around 12 °C)

$$= 1.3180 \times 10^{-4}$$

$$Ra_T^{(1)} = 899 \quad (\Delta T = 11.22\,^\circ\mathrm{C})$$

$$Ra_T^{(2)} = -1250 \quad (\Delta T = -15.60\,^\circ\mathrm{C}).$$

All these results suggest typical experiments using e.g. Laser-Doppler velocimetry to detect the onset of convection, and also to verify the wavenumber by recording the velocity component along the horizontal coordinate. Of course, one important remaining problem is to know which velocity component to measure and where to measure it, when watching for the onset of convection.

Normally, the type of experiments performed by Lhost and Platten [7] on water-alcohol systems could be repeated for the salt solution but, with small spacings like 2 or 3 mm, it is very unlikely that the vertical velocity could be recorded because the two laser beams would hit the lower and upper boundaries. There is of course no problem in measuring the horizontal velocity component V_x, but at which elevation z? Without the thermodiffusional effect $(\mathscr{D} = 0)$, the solution is symmetrical and one has to measure V_x at $z = 1/4$ or $3/4$. With the Soret effect, the solutions are no longer symmetrical. When $\mathscr{D} > 0$, the middle layer with its higher salt concentration rests on top of the bottom layer with its lower concentration. Thus convection should be stronger near the lower boundary than near the upper boundary. Thus, in order to

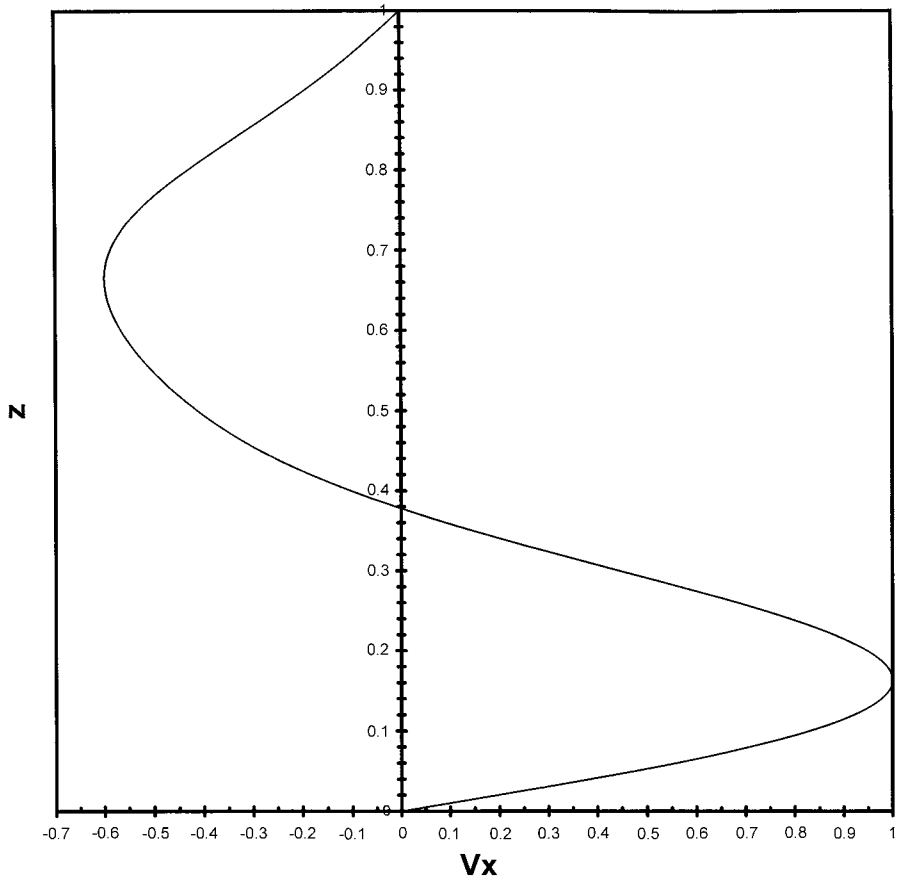

Fig. 4. Variation of the horizontal velocity V_x with elevation z.

correctly catch the onset of convection, one should have a good knowledge of the eigenfunctions of the linear problem. Computing the eigenvector (A_i, B_i, C_i), see Eqs. (43–45), we may construct W and, from the continuity equation, V_x, and therefore the streamlines. Results are given in Figure 4 for a very unsymmetrical case ($R_S \approx 330; Ra_T \approx -5000;\ Le = 140$), the goal being to show that V_x vanishes at $z = 0.38$ (instead of 0.5) and that it is preferable to measure V_x near the hot boundary around $z = 0.16$ (instead of $z = 1/4$ or $3/4$).

8. Conclusions

We have shown that a non-Boussinesq Soret effect with a zero mean Soret coefficient always destabilizes a two-component liquid layer, simply because there is in some part of the layer an unstable concentration stratification, independent of whether heating is from below or from above. This effect has been quantified using a linear hydrodynamic stability theory approach, and experiments are shown to be, if not easily achievable, at least possible. Hopefully such experiments will be undertaken in the not too distant future.

Acknowledgements

This paper presents results partly obtained in the framework of the Belgian programme on Interuniversity Poles of Attraction number 4–06 initiated by the Belgian State, Prime Minister's Office, Federal Office for Scientific, Technological and Cultural Affairs. The scientific responsibility is assumed by the authors.

References

[1] Caldwell, D. R., Measurement of negative thermal diffusion coefficients by observing the onset of thermohaline convection, J. Phys. Chem., 77 (1973), 2004–2008.

[2] Kolodner, P., Williams, H., Moe, C., Optical measurement of the Soret coefficient of ethanol/water solutions, J. Chem. Phys., 88 (1988), 6512–6524.

[3] Platten, J. K., Legros, J. Cl., Convection in Liquids, Springer, Berlin (1984).

[4] Chandrasekhar, S., Hydrodynamic and Hydromagnetic Stability, Oxford University Press, Oxford, 1961.

[5] Linz, S. J., Lücke, M., Convection in Binary Mixtures: A Galerkin model with impermeable boundary conditions, Phys. Rev. A, 35 (1987), 3997–4000; Non-Oberbeck-Boussinesq effects and barodiffusion in binary mixtures with small thermodiffusion ratio, Phys. Rev., A36 (1987), 3505–3508; Convection in binary fluid mixtures; traveling waves and lateral currents, Phys. Rev. A, 38 (1988), 5727–5741.

[6] a) Vergaftik, N. B., Handbook of Physical Properties of Liquids and Gases, Hemisphere Publishing Corp., Washington, 1983; b) Washburn, E. W., West, C. J., Dorsey, N. E., Eds., International Critical Tables of Numerical Data, McGraw-Hill, New York, 1928; c) Weast, R. C, Eds., Astle, M. J., Beyer, W. H., Eds., CRC Handbook of Chemistry and Physics, 67th Ed., CRC Press, Boca Raton, Florida, 1986–1987; Lide, D. R., Frederikse, H. P. R., Eds., 75th Ed., Special Student Edition, CRC Press, Boca Raton, Florida, 1913–1995.

[7] Lhost, O., Platten, J. K., Transition between steady states, traveling waves and modulated waves in the system water-isopropanol heated fom below, Phys. Rev. A, 38 (1988), 3147–3150; An experimental study of the transition from nonlinear traveling waves to steady overtuning convection, Phys. Rev. A, 40 (1989), 4552–4557; Study of large scale con-

vection induced by the Soret effect, Phys. Rev. A, 40 (1989), 6415–6420; Platten, J. K., Villers, D., Lhost, O., LDV study of some free convection problems at extremely slow velocities: Soret driven convection and Marangoni convection, in: Laser Doppler Anemometry in Fluid Mechanics, Vol. 3, Eds. R. J. Adrian, T. Asanuma, D. F. G Durao, F. Durst and J. H. Whitelaw, pp 245–260, Ladoan, Instituto Superior Technico, Lisbon, 1988.